Electronic Supplementary Information for:

Supramolecular self-assembled coordination architecture composed of a doubly bis(2-pyridyl)pyrazolate bridged dinuclear Cu^{II} complex and 7,7',8,8'-tetracyano-*p*-quinodimethanide radicals

Ryuta Ishikawa,*[a] Shunya Ueno[a], Hiroaki Iguchi,[b] Brian K. Breedlove,[b] Masahiro Yamashita[b,c,d] and Satoshi Kawata[a]

[a] Department of Chemistry, Faculty of Science, Fukuoka University, 8-19-1 Nanakuma, Jonan-ku, Fukuoka 814-0180, Japan.

[b] Department of Chemistry, Graduate School of Science, Tohoku University, 6-3 Aza-Aoba, Aramaki, Aoba-ku Sendai, Miyagi 980-8578, Japan.

[c] Advanced Institute for Materials Research (AIMR), Tohoku University, 2-1-1 Katahira, Aoba-ku, Sendai, Miyagi 980-8577, Japan.

[d] School of Materials Science and Engineering, Nankai University, Tianjin 300350, China.

Correspondence: ryutaishikawa@fukuoka-u.ac.jp

CrystEngComm

Table of Contents

Experimental details

Materials and methods

Copper(II) acetate monohydrate ($Cu(OAc)_2 \cdot H_2O$) and methanol (MeOH) were purchased from Wako Pure Chemical industries, Ltd.. 3,5-bis(2-pyridyl)pyrazole (Hbpypz) and 7,7',8,8'-tetracyano-*p*-quinodimethane (TCNQ) were purchased from Tokyo Chemical Industry (TCI) Co., Ltd.. TCNQ was purified by sublimation before use. All other chemicals were of reagent grade and used as received. LiTCNQ was prepared using a published procedure.[S1] All the synthetic reactions and manipulations were performed in the dark under aerobic conditions at room temperature.

Synthesis of $[Cu_4(\mu\text{-bpypz})_4(\mu\text{-TCNQ})_2](TCNQ)_2$ (**1**). A suitable crystal of **1** for single-crystal X-ray diffraction measurements was grown by using a liquid-liquid slow diffusion technique under an aerobic conditions at ambient temperature, wherein each reactant diffused in straight glass tubes that were 8 mm in diameter, leading to the growth of the crystals on the walls of the glassware. First, stock solutions of $Cu(OAc)_2 \cdot H_2O$ and Hbpypz and freshly prepared LiTCNQ were prepared separately in MeOH (20 mmol L^{-1}). Subsequently, 1.5 mL of the solution of $Cu(OAc)_2 \cdot H_2O$ and Hbpypz in MeOH was poured into the bottom of glass tube, and then 1.5 mL of the solution of freshly prepared LiTCNQ in MeOH was carefully layered on top of it. The glass tube was sealed and left undisturbed. Large dark green plate-shaped crystals suitable for single-crystal X-ray diffraction began to form after several days. The diffusion was complete in one week, accompanied by a little unidentified light green solid. Thus, the dark green crystals were separated from the glass tube carefully, washed with a small amount of cold MeOH, and dried in air to yield 49% of the product. Anal. Calc. for $C_{100}H_{52}Cu_4N_{32}$: C, 61.41; H, 2.68; N, 22.92. Found: C, 61.38; H, 2.47; N, 23.22. FTIR (KBr): ν_{CN} = 2191, 2180, 2166, 2159 cm^{-1} and ν_{CC} = 1503 cm^{-1}, and δ_{CH} = 825 and 817 cm^{-1}.

Single-crystal X-ray crystallography

A single crystal of **1** was coated with Nujol and quickly mounted on MicroLoops (MiTeGen Inc.) Data collection was performed with a Rigaku R-AXIS RAPID II IP diffractometer with graphite-monochromated Mo-Kα radiation (λ = 0.71075 Å) and a low-temperature device. Data integration, preliminary data analysis, and absorption collection were performed with the Rigaku CrystalClear-SM 1.4.0 SP1[S2] and CrystalStructure 4.2.2[S3] crystallographic software packages. The molecular structures were solved by the direct methods included in SIR92[S4] and refined with the SHELXL[S5] program. All non-hydrogen atoms were refined anisotropically. All the hydrogen atoms were included in the calculated positions. The lattice constants and structure refinement

parameters for **1** are summarised in Table S1.

Continuous wave electron paramagnetic resonance spectroscopy

Finely ground microcrystalline powders were sealed in quartz tubes of 4 mm diameter under N_2. CW X-band EPR spectra were recorded on a Bruker EMXmicro spectrometer equipped with a continuous flow liquid N_2 cryostat and a temperature controller. All the spectra were analysed with the Bruker Xenon software package. All the data were collected under the following experimental conditions: microwave frequency, ca. 9.433 GHz; microwave power, 2.20 mW; modulation amplitude, 4 G; modulation frequency, 100 kHz. Data measured at 170 K was simulated using the PHI program developed by Chilton et al.[S6]

Dc magnetic measurements

Magnetic data were collected with a Quantum Design MPMS XL-7 superconducting quantum interference device (SQUID) magnetometer. The measurements were performed with crushed crystalline samples in a calibrated gelatin capsule. Dc magnetic susceptibility measurements were performed in the temperature range of 2–300 K in a dc field of 1.0 T. Obtained magnetic susceptibility data were corrected for the diamagnetic contributions from the sample holder and core diamagnetism of each sample, which were estimated by using Pascal's constants.[S7]

Other physical measurements

Elemental analysis was performed on a Micro Corder JM10 (J-Science Lab Co., Ltd.). FTIR spectra were collected at room temperature on KBr disks using a JASCO FT/IR-410 spectrometer in the range of 400–4000 cm^{-1} and at a resolution of 4 cm^{-1}. Powder X-ray diffraction data was collected at room temperature with a RIGAKU MultiFlex diffractometer (50 kV/32 mA, 1.6 kW) with Cu-Kα radiation (λ = 1.5406 Å) in the 2θ range of 5–40° and a step width of 0.02°.

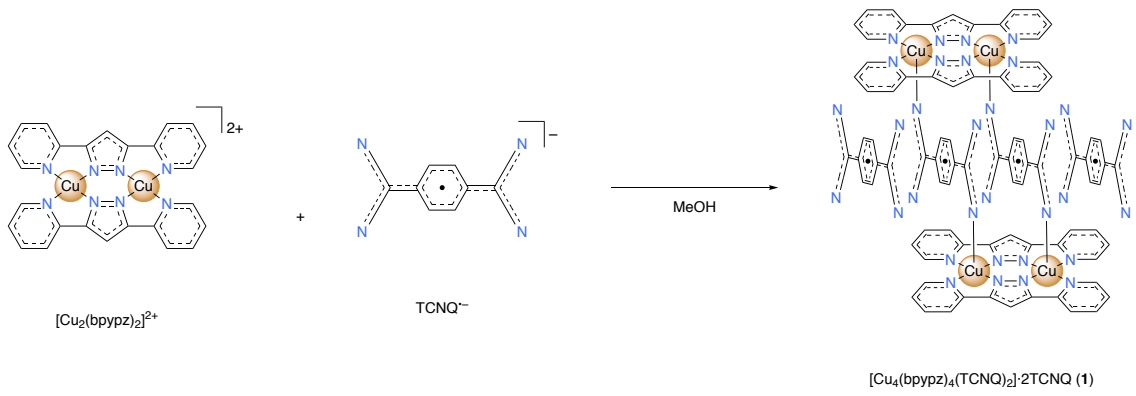

Scheme S1 Synthetic scheme of **1**.

Table S1 Single crystal X-ray crystallographic data for **1**.

	1
Empirical formula	$C_{100}H_{52}Cu_4N_{32}$
Formula weight (g mol^{-1})	1955.91
Crystal colour	Dark green
Crystal size (mm)	0.60×0.30×0.20
Temperature (K)	200
Crystal system	Monoclinic
Space group	$P2_1/c$ (No. 14)
a (Å)	14.2340(13)
b (Å)	19.8446(19)
c (Å)	15.4520(16)
α (°)	90
β (°)	106.326(3)
γ (°)	90
V (Å^3)	4188.7(7)
Z	2
F(000)	1984.0
Calculated density (g cm^{-3})	1.551
μ (mm^{-1})	1.076
R_1 (%)	4.33
wR_2 (%)	13.21
S	1.043

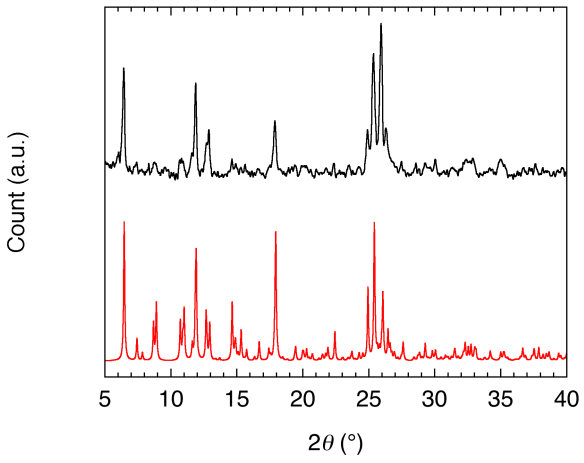

Fig. S1 Powder X-ray diffraction pattern for **1** (black) at room temperature and its calculated pattern (red) using single crystal X-ray diffraction data.

Table S2 Bond valence sum (BVS) analysis[a] for Cu centres within **1**. All bond distances are given in Å.

	$Cu–N_{pz1}$	$Cu–N_{pz2}$	$Cu–N_{py1}$	$Cu–N_{py2}$	$Cu–N_{TCNQ1}$	$Cu–N_{TCNQ2}$	BVS value	Assignment
Cu1	1.945(3)	1.949(3)	2.075(3)	2.091(3)	2.370(3)	2.997(4)	1.999(1.968)[b]	Cu^{II}
Cu2	1.945(3)	1.958(3)	2.078(3)	2.096(3)	2.282(3)	3.007(4)	2.023(1.993)[b]	Cu^{II}

[a] The BVS values are calculated using the following equations, $s_{ij} = \exp[(R_0 - r_{ij})/b]$ and $z_j = \Sigma s_{ij}$, where R_0 and b are empirical values of 1.713 Å for the Cu–N distance and 0.37 Å. r_{ij}, , s_{ij}, and z_j represent the interatomic distance between i and j, *i.e.*, the observed Cu–N bond distance, the bond valence for each Cu–N bond, and the BVS value, *i.e.*, the oxidation number of the Cu centre. [b] BVS values estimated as the five-coordinated geometry are also provided in parentheses.

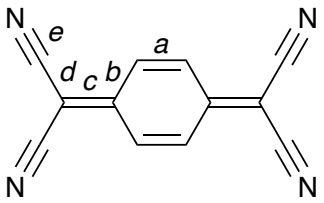

Scheme S2 Definition of bonds *a*–*e* on TCNQ.

Table S3 Key structural data (Å) used for analysis of charge (q) on TCNQ for **1** and standard reference compounds (TCNQ and RbTCNQ).

	Charge	*a*	*b*	*c*	*d*	*e*	q[a]	reference
TCNQ	0	1.346(3)	1.448(4)	1.374(3)	1.441(3)	1.140(1)	0	28
RbTCNQ	–1	1.373(4)	1.423(4)	1.420(4)	1.416(4)	1.153(4)	–1	28
1[b]		1.364(6)	1.422(6)	1.415(6)	1.422(6)	1.153(6)	–0.898	this work
		1.361(6)	1.422(6)	1.415(6)	1.425(7)	1.150(6)	–0.876	

[a] The q values are estimated using the following relationship, $q = -41.667[c/(b + d)] + 19.833$, where *b*–*c* represent bond distances indicated in Scheme S2. [b] Values measured at 200 K.

Table S4 Comparison of FTIR spectral data (cm^{-1})[a] for TCNQ, LiTCNQ, and **1**.

	ν_{CN}	ν_{CC}	δ_{CH}
TCNQ	2222	1542	861
LiTCNQ	2207, 2196, 2179, 2166	1508	826
1	2191, 2180, 2166, 2159	1503	825, 817

[a] All spectra were obtained for KBr pressed pellets.

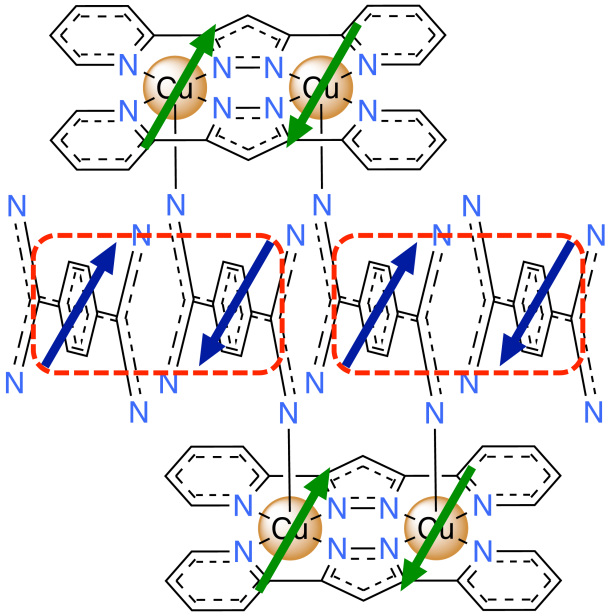

Scheme S3 Schematic representation with magnetic coupling exchange pathways in **1**.

Theoretical model of dc magnetic susceptibility data

A schematic representation with magnetic coupling exchange pathways for **1** is shown in Scheme S3. Face-to-face π-π stacked dimers, $(TCNQ^{\bullet-})_2$, in **1** contain a pair of very strongly antiferromagnetic coupled spins that give a diamagnetic ground state (surrounded by red frames). It should be noted that spins on $TCNQ^{\bullet-}$ do not significantly contribute to dc magnetic behaviour even at room temperature. Therefore, the dc magnetic data of **1** can be modelled with the following isotropic spin Hamiltonian for the sum of two noninteracting Cu^{II} dimers, $[Cu_2(\mu\text{-bpypz})_2]^{2+}$:

$$\hat{H} = -2\left(2J_{Cu1-Cu2}\hat{S}_{Cu1}\cdot\hat{S}_{Cu2}\right)$$

The analytical equation of the molar magnetic susceptibility can be estimated applying the van Vleck equation, which is known as the Bleaney-Bowers equation:

$$\chi_{\mathrm{M}} = (1-\mathrm{PI})\frac{4N_{\mathrm{A}}g_{\mathrm{av}}^2\mu_{\mathrm{B}}^2}{k_{\mathrm{B}}T}\left[\frac{1}{3+\exp\left(-\frac{2J_{\mathrm{Cu-Cu}}}{k_{\mathrm{B}}T}\right)}\right] + \mathrm{PI}\frac{4N_{\mathrm{A}}g^2\mu_{\mathrm{B}}^2}{3k_{\mathrm{B}}T}S_{\mathrm{Cu}}(S_{\mathrm{Cu}}+1) + \mathrm{TIP}$$

where N_{A}, g_{av}, μ_{B}, and k_{B}, represent the Avogadro number, the average Landé g factor, the Bohr magneton, the Boltzmann constant, respectively. In addition, the fraction of paramagnetic impurities (PI), and the temperature-independent paramagnetism (TIP) are included in the model, which is fixed at 60 × 10^{-6} cm^3 mol^{-1} per a Cu^{II} ion. The best fit of parameters were g_{av} = 2.11(1), $J_{\mathrm{Cu-Cu}}$ = –204.9(2) cm^{-1}, and PI = 3.3(2)% (R^2 = 0.9995).

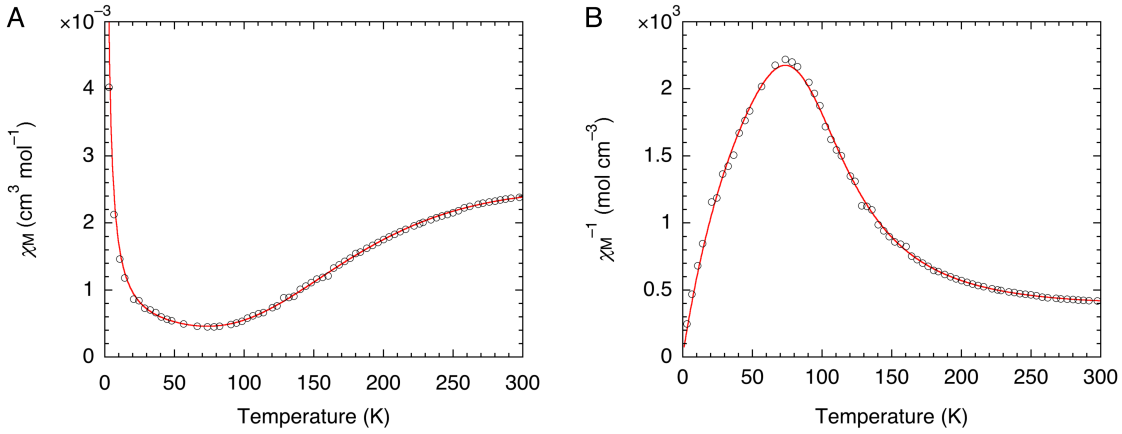

Fig. S2 Plots of χ_{M} versus temperature (A) and $1/\chi_{\mathrm{M}}$ versus temperature (B) for **1**. Fits using the spin Hamiltonian described in the Supplementary Information are represented by solid red lines.

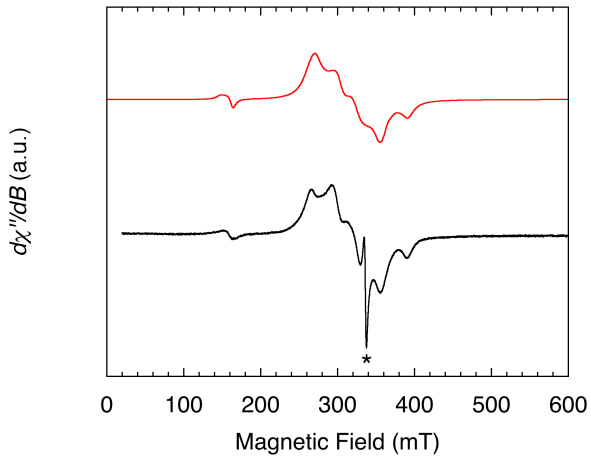

Fig. S3 CW X-band EPR spectrum for **1** at 170 K (black) and its simulation spectrum (red). The asterisk denotes a paramagnetic impurity of $TCNQ^{\bullet-}$ positioned at around g = 2.0031.

Theoretical models of CW X-band EPR spectrum

Each CW X-band spectrum showed features of thermally populated S = 1 signal of the antiferromagnetically Cu^{II} dimer, which was simulated according to the following zero-field splitting spin Hamiltonian:

$$\hat{H} = D\left(\hat{S}_z^2 - \frac{S(S+1)}{3}\right) + E\left(\hat{S}_x^2 - \hat{S}_y^2\right) + g\mu_B S\vec{B}$$

where respective terms correspond to the axial and rhombic zero-field splittings (D and E) and the Zeeman splitting. The best simulation of parameters were g_x = 2.28(1), g_y = 2.03(1), g_z = 2.03(1) (g_{av} = 2.11), D = –0.057(1) cm^{-1}, and E = 0.0028(6) cm^{-1} ($|E/D|$ = 0.0049) with z- and x,y-direction linewidths of 0.027(5) cm^{-1} and 0.017(7) cm^{-1}.

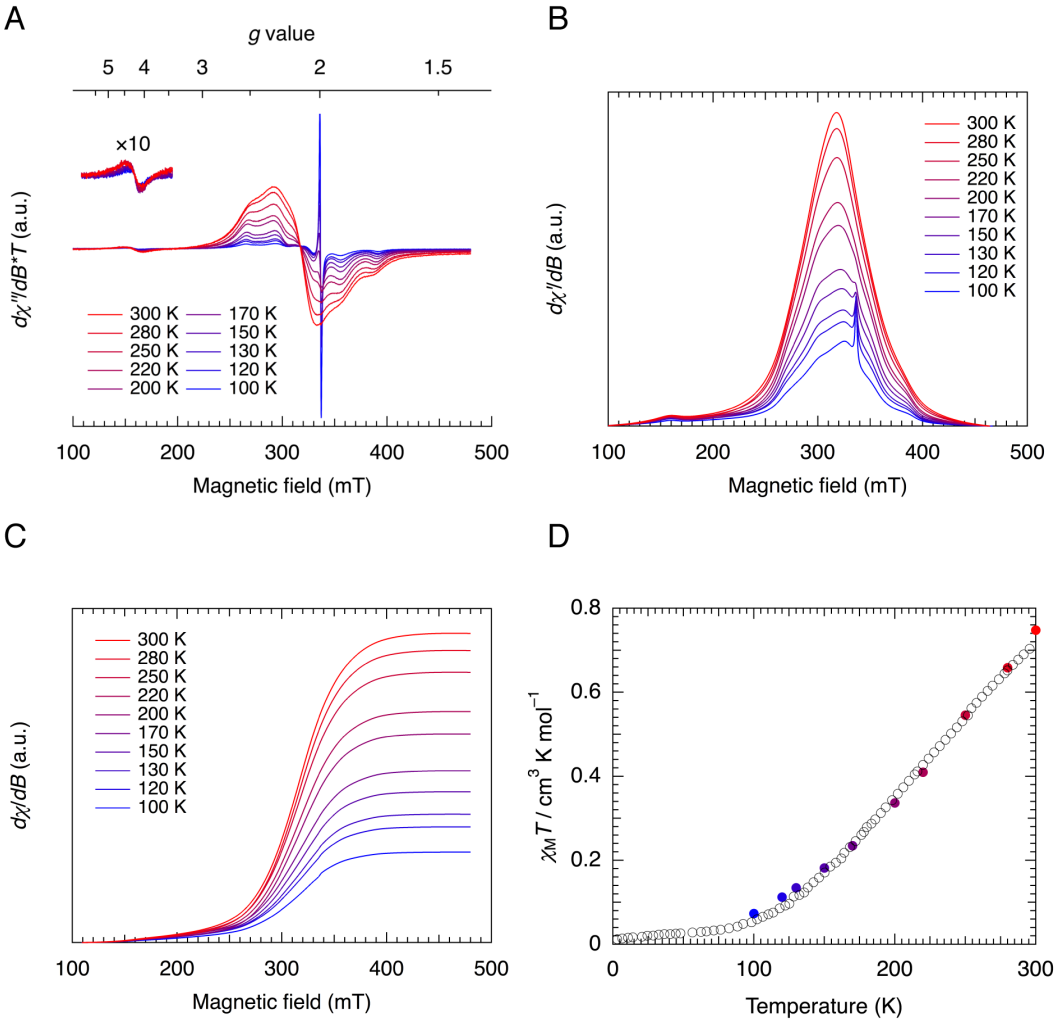

Fig. S4 (A) Variable-temperature CW X-band EPR spectra, (B) its first integration, (C) its second integration, and (D) plot of second integration times temperature versus temperature for **1**.

References

S1 L. R. Melby, R. J. Harder, W. R. Hertler, W. Mahler, R. E. Benson and W. E. Mochel, *J. Am. Chem. Soc.*, 1962, **84**, 3374–3387.

S2 *CrystalClear-SM; Version 1.4.0 SP1*: Rigaku and Rigaku/MSC, The Woodlands, TX, USA, 2008.

S3 *CrystalStructure Version 4.2.2*, Rigaku and Rigaku/MSC, The Woodlands, TX, USA, 2017.

S4 SIR92: A. Altomare, G. Cascarano, C. Giacovazzo, A. Guagliardi, M. C. Burla, G. Polidori and M. Camalli, *J. Appl. Crystallogr.*, 1994, **27**, 435.

S5 SHELXL: G. M. Sheldrick, *Acta Crystallogr.*, *Sect. C*: *Struct. Chem.*, 2015, **71**, 3–8.

S6 N. F. Chilton, R. P. Anderson, L. D. Turner, A. Soncini and K. S. Murray, *J. Comput. Chem.*, 2013, **34**, 1164–1175.

S7 G. A. Bain and J. F. Berry, *J. Chem. Educ.*, 2008, **85**, 532–536.